

LRP 790/04

November 2004

**Rapid and localized eITB formation  
during shear inversion in fully non-  
inductive TCV discharges**

M.A. Henderson, Y. Camenen, S.Coda,  
T.P. Goodman, P. Nikkola, A. Pochelon,  
O. Sauter and TCV Team

Accepted for publication in  
Phys. Rev. Letters

## Rapid and localized eITB formation during shear inversion in fully non-inductive TCV discharges

M.A. Henderson, Y. Camenen, S. Coda, T.P. Goodman, P. Nikkola, A. Pochelon, O. Sauter and TCV team  
*Centre de Recherches en Physique des Plasmas - École Polytechnique Fédérale de Lausanne,*  
*Association EURATOM-Confédération Suisse, CH-1015 Lausanne, Switzerland*  
 (Dated: August 11, 2004)

Clear evidence is reported for the first time of a rapid localized reduction of core electron energy diffusivity during the formation of an electron internal transport barrier (eITB). The transition occurs rapidly ( $\simeq 3ms$ ), during a slow ( $\simeq 200ms$ ) self-inductive evolution of the magnetic shear. This crucial observation, and the correlation of the transition with the time and location of the magnetic shear reversal, lend support to models attributing the reduced transport to the local properties of a zero-shear region, in contrast to models predicting a gradual reduction due to a weak or negative shear.

PACS numbers: 52.25.Fa, 52.55.Fi, 52.55.Wq, 52.50.Sw

The quest for fusion energy in magnetic confinement fusion devices has been plagued by anomalously high cross-field transport, which reduces the energy confinement by up to two orders of magnitude with respect to neo-classical theory, where energy transport is attributed to Coulomb collisions. However, transport barriers may arise within the plasma that improve the energy confinement. Two examples of such barriers are the H-mode [1] barrier located near the plasma edge, and the internal transport barrier (ITB) [2, 3] located in the plasma core. In a tokamak, a toroidal plasma current generates a poloidal magnetic field that combines with the larger toroidal magnetic field (supplied by external coils) to form helically twisted field lines that lie on closed and nested magnetic flux surfaces. The field lines are radially sheared, with the twist decreasing towards the outside in the normal configuration with the plasma current density profile ( $j_p$ ) peaked on axis. The magnetic shear ( $s$ ) is a quantity that measures the gradient in the reciprocal of the twist, and is thus generally positive. When  $j_p$  transforms from a peaked to a hollow profile,  $s$  flattens and then becomes negative in the center, forming an ITB in the process [4]. The barrier location has been observed both near and well inside the  $s=0$  flux surface [5]. Thus, there is an open debate on the mechanisms which improve the confinement associated with the ITB [6, 7]. For example, the weak or negative shear (WNS) theory attributes the formation of the barrier to a reduction in toroidal instabilities in regions with weak or negative shear [8–10]. The barrier strength should be proportional to the degree of negative shear implying that the barrier forms and evolves at the rate of the current profile evolution, and the barrier width extends over the plasma region with weak or negative shear. While the radial gap or Zero-Shear Gap (ZSG) theory [11] attributes the improved confinement to an increased spacing between resonant magnetic flux surfaces at the location of flat shear. The barrier should form only once a zero shear flux surface has been created in the plasma, with the appearance of the  $s=0$  surface acting as a formation threshold. The barrier should form rapidly and occupy a relatively

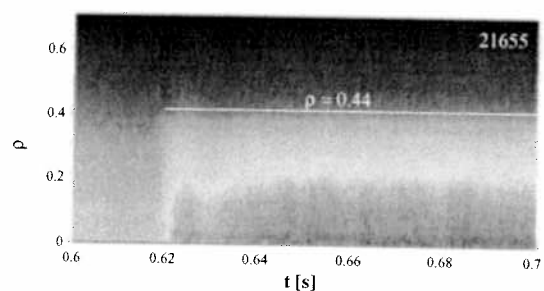


FIG. 1: The temporal evolution of the line-integrated soft x-ray emission across the plasma cross section. The eITB forms near 0.62s during a gradual evolution from a peaked to a hollow current density profile while keeping all external actuators constant.

small plasma region where  $s \simeq 0$ . Such contrasts in the expected barrier formation rate and width should be experimentally observable, however there has been no clear experimental evidence supporting any one theory despite the fact that ITBs have now been generated on several tokamaks [12].

In recent years the Tokamak à Configuration Variable (TCV), equipped with a 4.5MW electron cyclotron resonant heating (ECRH) system has made significant contributions in the realm of generation, sustainment and control of electron ITBs [13–17]. The ECRH system offers a set of highly localized independent heating and/or current drive (ECCD) sources that have been used to fully sustain the plasma current by distributing the EC beams across the plasma cross section [18] and, with regard to the eITB, tailor the driven current to generate and non-inductively sustain hollow current profiles. Even though the power density used to create and sustain these eITBs is impractical for direct application to a future reactor such as ITER, the control methodology [17] is extremely useful for studying the physics of the eITB. In particular, the eITBs can be formed during a gradual evolution from

peaked to hollow current profile at constant co-ECCD (colinear with the plasma current) injected power with no central heating. Such an example is shown in figure 1, where the transition to an eITB is observed near 0.62s on the temporal evolution of the line-integrated soft x-ray emission ( $I_{SX}$ ) measured by a multiwire chamber proportional x-ray detector (MPX) [19]. Everywhere inside of  $\rho \simeq 0.44$  (where  $\rho$  is a normalized radial coordinate proportional to the square root of the volume)  $I_{SX}$  is much higher than before the transition. Here, the change in  $I_{SX}$  reflects a change in the central electron temperature profile ( $T_e$ ), since the electron density profile ( $n_e$ ) is relatively constant ( $\Delta n_e \leq 7\%$ ) during the barrier formation. After the turn on of the co-ECCD power at 0.4s, all external actuators are held constant.

The generation of non-inductively driven eITBs on TCV initially starts with an ohmic plasma under stable conditions and  $j_P$  peaked on axis. The external electric field is then removed by holding the current in the ohmic transformer coil ( $I_{OH}$ ) constant at 0.4s, see figure 2a, and the plasma current is sustained using 1.0MW of co-ECCD deposited in the region  $0.25 < \rho < 0.4$ , which maintains the plasma current and broadens  $j_P$ . The co-ECCD current density profile ( $j_{CD}$ ), calculated using the Fokker-Planck quasilinear code CQL3D [20], is hollow or nearly flat from the deposition location inward due to particle diffusion [21]. The co-ECCD is also a heat source that broadens and increases  $T_e$ , steepens the electron pressure gradient off-axis ( $\nabla P_e$ ), and thus increases the bootstrap current ( $I_{BS}$ ). The bootstrap current density profile ( $j_{BS}$ ) [22] is peaked off-axis resulting in a hollow total  $j_P$  and a reversed magnetic shear profile. The eITB is obtained with the application of off-axis co-ECCD only: central heating or counter-ECCD (anti-parallel to the plasma current) can further improve performance [15, 17] but this phenomenology goes beyond the scope of this Letter.

The evolution of  $j_P$  from a peaked to a hollow profile occurs on a slow time scale due to the plasma self inductance, which generates local electric fields that drive currents ( $j_I$ ) inhibiting fast changes of  $j_P$ .  $j_I$  decays on a time scale governed by a combination of the plasma's L/R time constant ( $\tau_{L/R} \geq 200ms$ ) and the current redistribution time ( $\tau_{CRT} \leq 90ms$ ).  $\tau_{L/R}$  reflects the inductive nature of the plasma discharge as a whole, which inhibits change in the magnitude of the total driven current.  $\tau_{CRT}$  represents the time required for modifying a given  $j_P$  profile to a new profile, while keeping the total current constant and is estimated from the time evolution of the normalized internal inductance ( $\ell_i$ ), see figure 2b. The resulting evolution of  $j_P$  should occur on a time scale within the range of  $\tau_{CRT}$  and  $\tau_{L/R}$  depending on the difference between the ohmic and ECCD current profiles and magnitudes. The transition to a hollow profile is delayed until  $j_I$  has reduced and no longer fills the hollow current profile obtained from the combination of  $j_{CD}$  and  $j_{BS}$ .

Presently, there is no diagnostic that can measure the

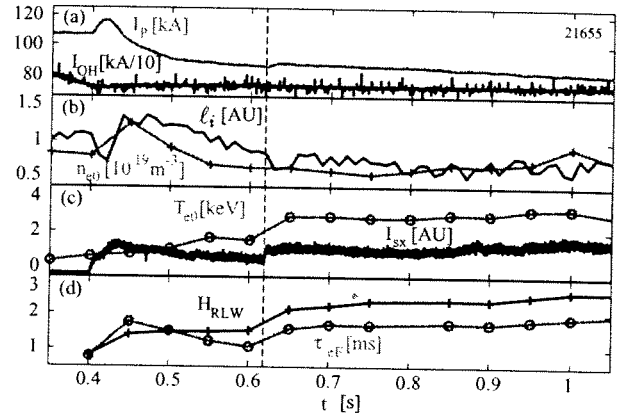


FIG. 2: Typical eITB discharge with the improved confinement starting at 0.62s, including (a) ohmic transformer coil current (blue) and plasma current (green); (b)  $\ell_i$  (blue) and central  $n_e$  (green), (c)  $I_{SX}$  (blue) and central  $T_e$  (green), and (d)  $H_{RLW}$  (blue) and  $\tau_{eE}$  (green).

$j_P$  profile on TCV, and therefore,  $j_P$  must be inferred from indirect measurements aided by modeling. The current density profile can be constructed from the sum of  $j_{CD}$ ,  $j_{BS}$  and  $j_I$  after  $t = 0.4s$  ( $t_1$ ) when the  $I_{OH}$  current is held constant.  $j_{BS}$  is calculated from  $T_e$  and  $n_e$  [22] measured by the Thomson Scattering (TS) system every 50 ms. The total EC-driven current is assumed to evolve in time as  $T_e/n_e$  measured at the co-ECCD deposition location, and the inductive current is assumed to decay exponentially starting at  $t_1$ : a fit to the measured total plasma current is then performed to determine the respective amplitudes of these currents and the  $j_I$  decay time  $\tau_{j_I}$ . Once these global parameters are determined, we turn our attention to the current density profiles. The profile shape of  $j_{CD}$  is supplied by CQL3D [21]. The  $j_I$  profile at  $t_1$ ,  $j_{I1}(\rho)$ , can then be calculated by subtracting  $j_{CD} + j_{BS}$  at  $t_1 + \delta$  (where  $\delta$  is a small time step) from the  $j_{BS} +$  Ohmic current density at  $t_1 - \delta$ ; the latter is in turn taken to be proportional to  $T_e^{3/2}$ , with the absolute amplitude constrained by the measured total current. Finally we can write  $j_I = j_{I1}(\rho) * e^{-(t-t_1)/\tau_{j_I}}$ . The modeled  $j_P$  becomes hollow between 0.6 and 0.7s consistent with the barrier formation near 0.62s, see figure 3. Although this is a simplified model of a complex evolution of  $j_P$ , the transition from a peaked to a hollow modeled  $j_P$  occurs consistently near the formation of the barrier for the five discharges analyzed.

Despite this slow evolution of  $j_P$  and  $s$ , the plasma confinement does not progress gradually, but experiences a sudden transition as revealed by the  $I_{SX}$  of figure 1 and 2c, with no measured change of MHD mode activity during this period. At the same time an increase occurs on  $T_e$ ,  $\tau_{eE}$  and the enhancement factor over TCV L-mode confinement [23], given by the Rebut-Lallia-Watkins scaling [24],  $H_{RLW} = \tau_{eE}/\tau_{RLW}$ , although the rapid formation is not discernable due to the relatively slow 20Hz

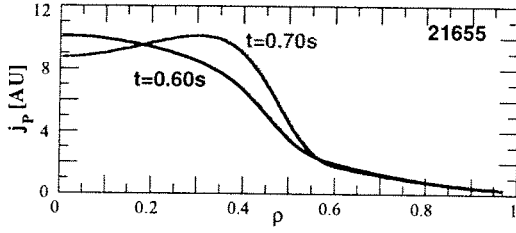


FIG. 3: Modeled  $j_P$  profiles for #21655 before (0.6s - blue) and after (0.7s - red) the eITB formation at 0.62s.

TS sampling rate. The sudden increase in  $I_{SX}$  of figure 1 is dominated by a rapid rise of the core  $T_e$ . The rapid barrier formation is clearly seen when plotting the temporal  $I_{SX}$  evolution of selected chords, see figure 4. At  $t \simeq 0.618s$ ,  $I_{SX}$  increases rapidly on chords viewing inside of  $\rho = 0.44$ , while  $I_{SX}$  on outer viewing chords register a momentary decrease indicating that a barrier has formed, which temporarily reduces the thermal flux from the core. The radial location between  $I_{SX}$ -chords with increasing and flat signals (dashed-dotted line of figure 4) corresponds to the barrier foot located near the barrier's radial position [25],  $\rho_{ITB} \simeq 0.43$  described by the radial location of the maximum value of  $\rho_T^*$  parameter [26]. The radial position of the barrier remains fairly constant, although the barrier strength [17] (associated with the maximum value of  $\rho_T^*$ ) gradually increases, consistent with a more reversed shear profile [27] as  $j_I$  continues to decrease.

The sudden increase in confinement indicates that a local threshold has been reached in the current profile evolution, leading to the formation of a barrier. Since the transition to a hollow  $j_P$  and the inversion of the shear-profile must occur sometime before 0.8s (when the current profile evolution has stabilized) and the model described above puts the time of transition from a peaked to hollow  $i_P$  within 50ms of the barrier formation, it is plausible to attribute the sudden increase in confinement with the appearance of a  $s=0$  surface off-axis. This behavior is consistent with the ZSG theory, where a sudden event, namely the appearance of a zero shear magnetic flux surface, results in the formation of a transport barrier, whereas it is contradictory to the WNS theory that would predict a gradual improvement in confinement on a  $j_P$  evolution time scale as the magnetic shear gradually becomes first weak and then negative.

The chord-integrated  $I_{SX}$  seems to indicate a uniform increase across the whole core; however, chords viewing the center cannot distinguish between an increase at the center and an increase near the barrier. A recently upgraded MPX camera, viewing the entire plasma cross section, is used to obtain a local emissivity profile ( $\epsilon_{SX}(\rho, t)$ ) by inverting the integrated profile, assuming a constant emissivity on a given flux surface and using a minimum Fisher inversion method [28]. The inverted profiles, averaged over 0.25ms and plotted at 0.75ms time intervals, are shown in figure 5a. The relative intensity (normal-

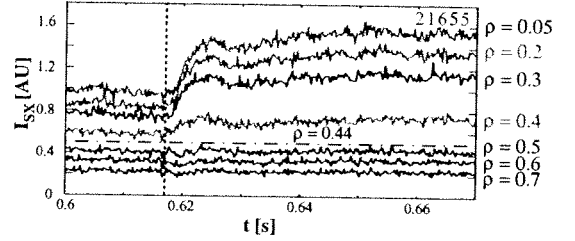


FIG. 4: The line-integrated  $I_{SX}$  viewed at selected values of  $\rho$ , during the eITB transition; the barrier foot position corresponds to the horizontal dashed-dotted line at  $\rho = 0.44$ .

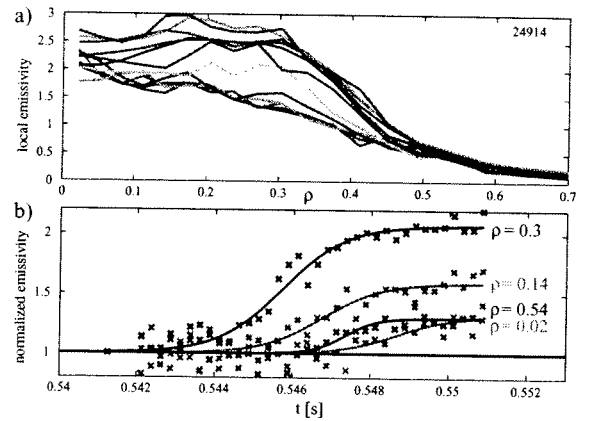


FIG. 5: (a) The reconstructed  $\epsilon_{SX}$  profiles averaged over 0.25s and plotted every 0.75ms during the eITB transition. (b) The temporal evolution of  $\epsilon_{SX}$  normalized and plotted for selected radial locations. The barrier forms first around  $\rho \simeq 0.3$ .

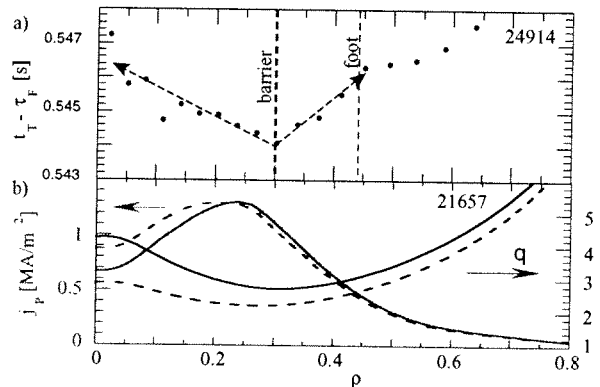


FIG. 6: (a) The fitted rise time ( $t_T - \tau_F$ ) of  $\epsilon_{SX}$ : the barrier forms at  $\rho \simeq 0.3$  (vertical dashed line) and the effects then propagate inward (blue line) and outward (green line). (b) Calculated  $j_P$  and  $q$ -profile from the CQL3D code for shot #21657 (equivalent to #21655 but in equilibrium conditions).

ized to pre-eITB levels) for selected radial locations may then be plotted as a function of time, see figure 5b. An increase in the soft x-ray emission is first observed in the region of  $\rho \simeq 0.3$ , then progresses inward toward the center and outward toward the barrier foot. We chose to estimate the propagation time by fitting (solid line) the relative intensity change at each radial position to a hyperbolic tangent:  $\Delta\epsilon(\rho)\tanh[(t - t_T(\rho))/\tau_F(\rho)]$ . Where  $\Delta\epsilon(\rho)$  corresponds to the amplitude rise,  $t_T(\rho)$  the inflection point of the rise and  $\tau_F(\rho)$  the rise time for the given flux surface  $\rho$ . The time of the initial rise of  $\epsilon_{SX}$  at each radial location is approximated by  $t_T(\rho) - \tau_F(\rho)$ , and is plotted as a function of  $\rho$  in figure 6a. The increase in  $\epsilon_{SX}$  occurs first at  $\rho \simeq 0.3$ , which can be attributed to a local decrease in thermal diffusivity, i.e. the formation of a barrier. As time progresses, neighboring flux surfaces are influenced as the barrier ‘dams’ the thermal flux resulting in a build up of the central temperature. The inward and outward propagating effects of the barrier formation of figure 6 results in a relatively sharp ‘V’ rather than a ‘U’ shape indicating that the barrier width is very narrow  $\leq 0.05$  in  $\rho$  (or 1.2cm). The flat  $T_e$  profiles typical of the region contained inside eITBs [5, 15] also indicates that the diffusivity is comparably higher inside  $\rho < 0.3$  than at the barrier. The barrier is located at the edge of the  $\epsilon_{SX}$  or  $T_e$  flat top and not farther out at  $\rho_{ITB}$  [25] near the  $T_e$  inflection point nor at the barrier foot ( $\rho \simeq 0.44$  of figure 4) characterized by the radial location of unchanging  $I_{SX}$ -chords.

The  $j_P$  (red curves) and q-profiles (blue curves) were calculated using CQL3D, see figure 6b, for shot #21657 once an equilibrium was achieved (usually central heating is added before equilibrium is achieved). The calculations assumed two different averaged effective charge values,  $Z_{eff} = 5$  (solid) and 2.5 (dashed). In each case the diffusion coefficient (D) was chosen in such a way as to best reproduce the experimental total plasma current, e.g.  $D = 0.5m^2/s$  (solid) and  $0.7m^2/s$  (dashed)

[29]. In both cases the zero-shear flux surface occurs near  $\rho \simeq 0.3$ , equivalent to the barrier location  $\rho_B \simeq 0.3$  of figure 6a. Since the barrier location corresponds to the modeled  $s=0$  and that the barrier position remains stable, it is reasonable to hypothesize that the threshold corresponds to the appearance of a zero-shear ( $s=0$ ) magnetic flux surface, where the barrier forms when and where  $s = 0$ . Here we have not invoked anything other than a local increase in confinement at a radial position corresponding to  $s = 0$  to explain the experimental data. A rigorous experimental confirmation of this hypothesis, however, requires diagnostics that are currently unavailable on TCX.

In conclusion, experimental results show that the transition from L-mode to an eITB occurs on a very rapid time scale  $\leq 3ms$  during a slow evolution of the current density profile occurring over 200ms, from a well-defined peaked inductive ohmic profile to a steady-state fully non-inductively sustained hollow profile, at constant input power. Furthermore, the barrier forms in a very narrow region off-axis that is consistent with the radial location of the zero shear magnetic flux surface, at the time at which the current density becomes hollow. These new experimental results provide a unique test for validating theories on internal transport barriers, which must account for the rapid and localized barrier formation.

#### Acknowledgments

The authors would like to acknowledge Basil Duval who helped greatly in proof reading and in numerous discussions concerning the organization of this manuscript. Also, Roland Behn and Ge Zhuang are to be acknowledge for their work with the TS diagnostic and Alexei Sushkov for his work with the MPX. This work was supported in part by the Swiss National Science Foundation.

- 
- [1] F. Wagner *et al*, Phys. Rev. Lett. **49** (1982) 1408.
  - [2] F.M. Levinton *et al*, Phys. Rev. Lett. **75** (1995) 4417.
  - [3] E.J. Strait *et al*, Phys. Rev. Lett. **75** (1995) 4421.
  - [4] C.M. Greenfield *et al*, Phys. Plasmas **4** (1997) 1596.
  - [5] T. Fujita *et al*, Nucl. Fusion **39** (1999) 1627.
  - [6] J. Candy *et al*, Phys. Plasmas **11** (2004) 1879.
  - [7] K. Garbet *et al*, Phys. Plasmas **8** (2001) 2793.
  - [8] E. Waltz *et al*, Phys. Plasmas **2** (1995) 2408.
  - [9] J.F. Drake *et al*, Phys. Rev. Lett. **77** (1996) 494.
  - [10] M. Beer *et al*, Phys. Plasmas **4** (1997) 1792.
  - [11] Y. Kishimoto *et al*, Nucl. Fusion **40** (2000) 667.
  - [12] R.C. Wolf, Plasma Phys. Contr. Fus. **45** (2003) R1 and references therein.
  - [13] S. Coda *et al*, Plasma Phys. Contr. Fus. **42** (2000) B311.
  - [14] Z.A. Pietrzyk *et al*, Phys. Rev. Lett. **86** (2001) 1530.
  - [15] O. Sauter *et al*, Proc. 29th EPS Conf. on Contr. Fus. and Plasma Phys., ECA **26B** (2002) P2-087.
  - [16] T.P. Goodman *et al*, Nucl. Fusion **43** (2003) 1619.
  - [17] M.A. Henderson *et al*, Plasma Phys. Contr. Fus. **46** (2004) A275.
  - [18] O. Sauter *et al*, Phys. Rev. Lett. **84** (2000) 3322.
  - [19] A.V. Sushkov *et al*, Proc. 29<sup>th</sup> EPS Conf. on Contr. Fus. and Plasma Phys., ECA **26B** (2002) P4-118.
  - [20] R.W. Harvey and M.G. McCoy, Proc. IAEA TCM (Montreal, 1992).
  - [21] P. Nikkola *et al*, Nucl. Fusion **43** (2003) 1343.
  - [22] O. Sauter *et al*, Phys. Plasmas **6** (1999) 2834.
  - [23] A. Pochelon *et al*, Nucl. Fusion **39** (1999) 1807.
  - [24] P.H. Rebut *et al*, Proc. 12<sup>th</sup> Int. Conf. of Plasma Phys. and Cont. Fusion Res., **2** (IAEA, Vienna, 1989) p.191.
  - [25] B. Esposito *et al*, Plasma Phys. Contr. Fus. **45** (2003) 933.
  - [26] G. Tresset *et al*, Nucl. Fusion **42** (2002) 520.
  - [27] M.A. Henderson *et al*, Phys. Plasmas **10** (2003) 1796.
  - [28] M. Anton *et al*, Plasma Phys. Contr. Fus. **38** (1996) 1849.
  - [29] P. Nikkola, EPFL Thesis No. 3048 (2004).